Laser and GTAW torch processing of Fe-Cr-B coatings on steel: II- microstructure and hardness

A.N. Md Idriss[1], S. Mridha[*1] and T.N. Baker[2]

[1]Advanced Materials and Surface Engineering Research Unit

Department of Manufacturing and Materials Engineering

International Islamic University of Malaysia, P.O. Box 10, 50728, Kuala Lumpur, Malaysia

[2]Department of Mechanical and Aerospace Engineering, James Weir Building

University of Strathclyde, Glasgow G1 1XJ, UK

[1]ahmednazrin@gmail.com; [*1]shahjahanmridha@gmail.com; [2]neville.baker@strath.ac.uk

*Corresponding author, present address: Department of Mechanical and Aerospace Engineering, James Weir Building, University of Strathclyde, Glasgow G1 1XJ, UK

ABSTRACT

A comparison has been made of the relationship between microstructure and microhardness developed by surface melting Nanosteel SHS 7170 Fe-Cr-B alloy powder onto a plain carbon steel surface. This powder was initially developed as a high velocity oxy fuel sprayed coating giving a strength ten times that of mild steel, and is particularly suitable for surface protection against wear and corrosion. In this study, the alloy powder was injected into the laser melted surface, while a preplaced powder was melted using the gas tungsten arc welding (GTAW) technique. The laser track consisted of fine dendrites and needle-like microstructures which produced a maximum hardness value of over 800 HV, while the GTAW track produced a mixture of equiaxed and columnar grain microstructures with a maximum hardness value of

670 HV. The lower hardness values are considered to be associated with dilution and grain size.

Keywords: Coating, Steel, Fe-Cr-B powder, Laser, GTAW torch, Microstructure, Hardness.

1 INTRODUCTION

Laser coating substrates such as aluminium, steels and titanium is known to improve the wear and corrosion resistance compared to the untreated substrate.[1, 2] The process generates a quality coated layer having minimal distortion and a small geometric dilution. But the technique involves a high cost of equipment and is relatively uneconomical due to the slow processing speed.[3-5] For some applications, laser processing is unfavourable for total surface coating. An alternative, developed from gas tungsten arc welding (GTAW) has been found to be adequate for modifying the surface layer of the base metal, [6-10] but this method generates a large geometric dilution. Three comparisons between GTAW and laser coating techniques have been undertaken previously. Xu et al[11] reported that following coating a Co based alloy powder onto a SUS403 stainless steel base metal, the dilutions for the diode laser cladded samples were 4 and 7%, using output powers of 500 and 600 W, respectively. On the other hand, the GTAW samples produced dilutions of 41 and 46% with heat inputs of 12~15 kJ cm^{-1} (100 and 120 A). In other work, Kaul et al., [12] studying the microstructure of a 1.2 mm thick sheet of stabilized 17 wt-% Cr stainless steel, observed columnar grains growing from the resolidified melt front to meet the axial grains at the centerline after both GTAW and CO_2 laser melting. The microhardness values for both GTAW and laser processed samples ranged from 200 to 230 HV(100 g) and 245 to 270 HV(100 g), respectively. Using a 40CrMnMo7(1.2311) tool steel as the base metal and filler wire, Vedani [13] found that the

hardened layer produced on a Nd-YAG laser melted sample was 300 μm in thickness, while it was 10 times deeper for the GTAW track. In two of these studies, stainless steel surfaces were modified either with or without adding Co based alloy powder, while in the third case, a tool steel substrate was used employing a tool steel powder.

The Nanosteel SHS 7170 powder used in this work is a multicomponent alloy system with a high glass forming ability (GFA) and is known to be particularly suitable for surface protection against wear and corrosion.[14, 15] The nanoscale microstructure of ~100 nm in diameter, possessed by the SHS 7170 gas atomized powder, is reported to provide a unique combination of high hardness and toughness, giving a strength ten times that of conventional steel.[16] A very limited amount of work has been reported previously on the use of this alloy powder which was developed as a high velocity oxy fuel (HVOF) sprayed coating.[17-19]

The motivation for this work was to explore the suitability and understand the relationships between microstructure and microhardness in the coatings of the Fe-Cr-B alloy powder for use in surface engineering a mild steel substrate using processes other than HVOF. Two techniques were compared, each with two sets of conditions: (a) melting preplaced SHS 7170 alloy powder on a steel surface using a conventional GTAW torch, and (b) processing by powder injection into a laser melted steel surface. The melt features of the Fe-Cr-B alloy coating produced on plain carbon steel using both laser and GTAW surface engineering techniques were compared in part I, [20] while in this paper (part II), relationships between the microstructure and hardness development in the re-solidified tracks are considered.

2 EXPERIMENTAL

A coaxial YLR-2000 ytterbium fiber laser with a wavelength at 1070 nm and a single phase GTAW machine type TIG165 were used to produce the coated samples under the processing

conditions, which are given in Tables 1 and 2, respectively. SHS 7170 gas atomized Fe-Cr-B alloy powder was used as the reinforcing material to produce single tracks on the mild steel (BS08015) substrate surface. The full chemical composition provided by the manufacturer is 18-22Cr, 3.9-7Mo, 5-6.5W, 2-4.9Mn, 0.3-1.9Si, 3-4B, and <0.4C (all in wt-%) with a nominal size in the range of 15 to 53 μm.

Metallographic specimens from the track vertical cross sections were prepared using a standard technique and polished cross-sections were etched with acidic ferric chloride solution (25 g of $FeCl_3$, 25 mL of HCl and 100 mL of distilled water). Further details of the experiment work and substrate are described in part I. [20]

A JEOL JSM 5600 scanning electron microscope was used to study the microstructure and a Wilson Wolpert microhardness testing machine was used to determine the hardness of the samples at 200 gf with 10 s delay. An average of three readings was used. The error in the microhardness data was ±5 HV. The heat inputs for the laser and GTAW processing were calculated using standard expressions from literature; [19, 22, 23] for laser processing, $E = P/sD$, where P is the laser power, s scanning speed or the velocity of the work-piece and D is the diameter of the laser spot: for GTAW processing, $E = \eta VI/s$, where V is voltage, I is current, s is scanning speed and η is efficiency of energy absorption, which was 48%. Details of the processing conditions, calculated energy inputs and dilutions for the melted tracks are given in Tables 1 and 2. It is to be noted that the coupling factor of laser beam is influenced by the substrate material and any powder injected during melting. Because of uncertainty this factor has not been considered here in calculating the laser energy.

3 RESULTS AND DISCUSSION

3.1 Microstructure

A re-solidified layer formed after the powder, which had melted, alloyed with the molten substrate layer. The melt cross-sections of both laser processed tracks and GTAW tracks were hemispherical in shape, as described in part I [20], and have also been observed previously. [24-27] The variation in geometric dilution was reflected in the development of the microstructure, composition and hardness in the coatings produced by the two surface melting techniques.

Following laser processing, the geometric dilution is relatively low, as seen in Table 1, while after melting using the GTAW processing technique, is very high because of the high heat input, Table 2.

The microstructure at the central region of the 125 J mm^{-1} laser processed track consisted of equiaxed dendrites, Fig. 1a with traces of all elements of the alloy powder present in the EDX spectrum (Fig. 1b). Also, these processing conditions produced columnar dendrites, seen in Fig. 1c. In the coating processed by the laser with 188 J mm^{-1} heat input, the microstructure consisted of needle-like dendrites at the central region of the melt pool, Fig. 2a. The EDX analysis from this region in Fig. 2b shows a higher chromium concentration compared to that of Fig. 1b, suggesting a decreased dilution under this processing condition. At the re-solidified melt front, an interdendritic microstructure between the needle- like dendrites and columnar dendrites was observed, Fig. 2c. This suggests that the columnar dendrites have grown from the melt matrix interface against the direction of heat flow, while needle-like dendrites grew towards the heat source. The columnar dendrites in Fig. 2c are very small compared to those in the track processed at 188 J mm^{-1}, Fig. 1c.

No martensitic microstructures were observed in the melt pool of any of the laser tracks. However, the HAZs of both laser and GTAW tracks consisted mainly of martensitic microstructures.

The faster specimen speed associated with the 125 J mm^{-1} energy, Table 1, which allowed only a short time for powder injection, resulted in a smaller powder volume delivered into the melt. This generated a having a high fluidity, which took a long time to solidify. The result was the formation of with large columnar dendrites at the melt front and an axial microstructure ahead of this columnar structure (Fig. 1). The higher volume of injected powder associated with the 188 J mm^{-1} track was believed to have produced a lower temperature melt than that using 125 J mm^{-1}. Upon fast freezing, this resulted in smaller dendrites (Fig. 2), which were about 40 µm long, compared to 100 µm long dendrites after the 125 J mm^{-1} processing (Fig. 1). A greater dimensional dilution in the 125 J/mm track (Table 1) was the overwhelming consequence of the reduction of elements, particularly of chromium in Fig. 1b compared to the low speed laser track produced at 188 J/mm (Fig. 2b).

The microstructures in Figs. 1c and 2c show a planar crystallization at the interface, which means the formation of a good metallurgical bonding between the coating and the base metal. From the interface to the centre of the melt pool, cellular and dendritic solidification occurred in an opposite direction to the heat flux. Planar crystallization has been reported at the interface; subsequently dendrites in the coated layer grow epitaxially along the direction of heat flow towards the center of the re-solidified melt pool. [28]

A consideration of the GTAW tracks, which were processed at 1008 and 1296 J mm^{-1} energy inputs, showed that the microstructures consisted of columnar grains at the melt front and equiaxed grains in the central region of the melt; the columnar grains grew from the melt interface. Compared to grains of the 1008 J mm^{-1} track seen in Fig. 3, the 1296 J mm^{-1} track produced coarser grains, Fig. 4. The average width and length of the columnar grains were 9 and 28 µm, for the 1008 J mm^{-1} track and 14 and 43 µm, for the 1296 J mm^{-1} track, respectively. By comparison, the diameters of the equiaxed grains were 13 and 18 µm for the

1008 and 1296 J mm^{-1} tracks, respectively. Variations in the melt temperature and solidification rate are considered to be responsible for the generation of the coating microstructures having grains of different dimensions.

Gas tungsten arc melting processing induced a greater dimensional dilution and melting of the Fe-Cr-B powder than laser processing. This created a vigorous mixing and hence the concentration of alloying elements was significantly lower (Figs. 3b and 4b) than those of the laser tracks (Figs. 1b and 2b). The cooling rate, which was higher in the laser tracks, has a profound effect on the melt composition and microstructure.

With GTAW processing, it is considered that a faster cooling rate occurred following an energy input of 1008 J mm^{-1} compared to the 1296 J mm^{-1}. This resulted in less time for the elemental segregation and solidification, leading to the formation of a small grain microstructure as seen in Fig. 3. The longer solidification period after the 1296 J mm^{-1} processing, was associated with larger grains, Fig. 4. A similar explanation concerning the variation in grain size of the microstructure has been reported previously.[11]

3.2 Microhardness

The hardness depth profiles of the melt cross- sections presented in Fig. 5 show greater hardness values in laser tracks than those in GTAW tracks. The maximum hardness of the laser track processed at 125 J mm^{-1} is 790 HV compared to 880 HV in the 188 J mm^{-1} track. The higher hardness found in the 188 J mm^{-1} track is considered to be related to the smaller size of dendrites as seen in Fig. 1a. The greater volume of powder delivery in the higher energy 188 J mm^{-1} track produced a lower temperature melt which resulted in a faster cooling and also a lower dimensional dilution of 41%, compared to that in the 125 J mm^{-1} track (Table 1). The high hardness developed in the coating layer was retained to a depth of 560 µm and then reduced sharply to the base hardness of about 180 HV. A thin layer with a

hardness about 430 HV followed the melt layer for all tracks, which is the HAZ. A similar hardness development in laser tracks was reported by others.[29]

In the GTAW tracks, the average hardness values ranged from 588 HV for 1296 J mm^{-1} processing to 670 HV at 1008 J mm^{-1}, retained to respective melt depths of 1.80 mm and 1.30 mm. The lower hardness (588 HV) of the 1296 J mm^{-1} GTAW track may be related to its coarser microstructure, as seen in Fig. 4, compared to finer microstructure of the 1008 J mm^{-1} track with higher hardness values (Fig. 3). Compared to the base metal hardness of 180 HV, that in the laser tracks was 4 to 5 times greater, while that in the GTAW tracks increased by 3 to 4 times. It is to be noted that according to the manufacturer's specification, the Nanosteel powder hardness falls within the range 900 to 1100 HV. Therefore, the maximum hardness of the coatings produced in this work are lower than the hardness of the Nanosteel powder, and dimensional dilution is considered to be responsible for development of these lower hardness regions. The 1008 J mm^{-1} GTAW track with 87% dilution (Table 2) has hardness of 670 HV, which reduced to 588 HV when dilution was 95% after melting at 1296 J mm^{-1}. Similarly the laser track with 41% dilution processed with an energy input of 188 J mm^{-1} had a maximum hardness of 880 HV, which decreased to 790 HV when dilution increased to 63% after melting at 125 J mm^{-1} energy input. The results of the present investigation are in agreement with the work of Colaco et al.[29] The hardness of coating layer was affected primarily by dilution and secondly by microstructure, especially that associated with the size of dendrites. Li et al.[30] also observed that the hardness values of coatings are primarily affected by the dimensional dilution followed by dendrite structures.

4 CONCLUSIONS

The investigation on microstructure and hardness of Fe-Cr-B powder coatings on plain carbon steel processed by laser and GTAW surface engineering techniques revealed that:

- The microstructure of the laser tracks consisted mainly of dendrites. The 125 J mm^{-1} track produced columnar and equiaxed dendritic microstructure, while the 188 J mm^{-1} track had a more needle-like microstructure. The microstructure of the GTAW tracks consisted of columnar grains at the melt front and axial grains at the melt center; the grains were larger with the higher energy input.
- Compared with the base metal hardness of 180 HV, the maximum hardness developed in the laser tracks was 4 to 5 times greater, but only 3 to 4 times more in the GTAW tracks. Compared to the 188 J mm^{-1} laser track, the hardness was lower in the 125 J mm^{-1} track, while a higher hardness was achieved by the low energy melting (1008 J mm^{-1}) in GTAW tracks. Large geometric dilution is considered to be partially responsible for the reduced hardness development in both laser and GTAW processing.
- The processing conditions for both laser and GTAW techniques require optimization to achieve the maximum hardness levels attainable using Nanosteel SHS 7170 Fe-Cr-B alloy powder.

ACKNOWLEDGEMENT

The authors would like to thank the Department of Mechanical, Materials and Manufacturing Engineering, Nottingham University, United Kingdom for providing laser and laboratory facilities.

REFERENCES

[1] J. C. Ion 'Laser Processing of Engineering Materials', 2005, Elsevier, Amsterdam.

[2] H. Dong (Ed.), 'Surface Engineering of Light Alloys - Aluminium, Magnesium and Titanium Alloys', 2010, Wood Publishing Ltd, Oxford.

[3] A. K. E. Toyserkani and S. Corbin: 'Laser Cladding', 2005, CRC Press LLC, Florida.

[4] C. Pfohl and K. T. Rie: 'Wear-resistant PACVD coatings of the system Ti-B-N', Surf. Coat. Technol., 1999, **116-119**, 911-915.

[5] J. Oh, S. Lee: 'Correlation of microstructure with hardness and fracture properties of (TiC,SiC)/Ti-6Al-4V surface composites fabricated by high-energy electron-beam irradiation', Surf. Coat. Technol., 2004, **179**, 340-348.

[6] S. Mridha, H.S. Ong, L.S. Poh and P. Cheang: 'Intermetallic coatings produced by GTAW surface melting', J. Mater. Process. Technol., 2001, **113**, 516-620.

[7] S. Buytoz, M. Ulutan and M.M. Yildirim: 'Dry sliding wear behavior of GTAW welding clad WC composite coatings', Appl. Surf. Sci., 2005, **252**, 1313-1323.

[8] D. Wenbin, J. Haiyan, Z. Xiaoqin, L. Dehui and Y. Shoushan: 'Microstructure and mechanical properties of GTA surface modified composite layer on magnesium alloy AZ31 with SiC_P', J. Alloys Compd., 2007, **429**, 233-241.

[9] S. Mridha: 'Titanium nitride layer formation by TIG surface melting in reactive environment', J. Mater. Proc. Technol., 2005, **168**, 471-477.

[10] S. Mridha, A.N.Md Idriss, M.A. Maleque, Suryanto and Souad A.: 'Effect of voltage on the consolidation of TiC particulates on steel substrate fused by TIG welding arc', IJMME, 2012, **7(1)**, 48-53.

[11] G. Xu, M. Kutsuna, Z. Liu and K. Yamada: 'Comparison between diode laser and GTAW cladding of Co-based alloys on the SUS403 stainless steel', Surf. Coat. Technol., 2006, **201(3-4)**, 1138-1144.

[12] R. Kaul, P. Ganesh, P. Tripathi, R.V. Nandedkar and A.K. Nath: 'Comparison of laser and gas tungsten arc weldments of stabilized 17 wt-%Cr ferritic stainless steel', Mater. Manufac. Process., 2003, **18(4)**, 563-580.

[13] M. Vedani: 'Microstructural evolution of tool steels after Nd-YAG laser repair welding', J. Mater. Sci., 2004, **39(1)**, 241-249.

[14] K. Chokethawai: 'Microstructural evolution in Fe-Cr-B based alloy powder and thermally sprayed coatings and their wear performance', 2010, PhD Thesis, University of Nottingham, United Kingdom.

[15] D.J. Branagan: 'Development of Nanostructured Coatings for Enhanced Corrosion Performance', Adv. Mater. Process., 2011, **169 (2)**, 33-34.

[16] Available from: http://nanosteelco.com/.

[17] K. Chokethawai, D.G. McCartney and P.H. Shipway: 'Microstructure evolution and thermal stability of an Fe-based amorphous alloy powder and thermally sprayed coatings', J. Alloy Comp., 2009, **480(2)**, 351-359.

[18] V.K. Balla and A. Bandyopadhyay: 'Laser processing of Fe-based bulk amorphous alloy', Surf. Coat. Technol., 2010, 205**(7)**, 2661-2667.

[19] M. Schneider: 'Laser cladding with powder, effect of some machining parameters on clad properties', 1998, PhD Thesis, University of Twente, Enschede, The Netherlands.

[20] A.N. Md Idriss, S. Mridha and T.N. Baker: 'Laser and GTAW torch processing of Fe-Cr-B coatings on steel: I- melt features', Mater. Sc. Technol., in press, 2013, DOI 10.1179/1743284713Y.0000000435.

[21] E. Schubert, T. Seefeld, A. Rinn and G. Sepold: 'Laser beam cladding: A flexible tool for local surface treatment and repair', J. Therm. Spray Technol., 1999, **8(4)**, 590-596.

[22] K.E. Easterling: 'Introduction to Physical Metallurgy of Welding', Butterworth-Heinemann, 1992, London.

[23] S. Mridha and T.N. Baker: 'Metal matrix composite layer formation with 3 micron SiCp powder on IMI318 titanium alloy surfaces through laser treatment', J. Mater. Process. Technol., 1997, **63**, 432-437.

[24] S. Mridha and B.S. Ng: 'Addition of ceramic particles to GTAW melted titanium surfaces', Surf. Eng., 1999, **15(3)**, 210-215.

[25] S. Mridha and T.N. Baker: 'Incorporation of 3 μm SiCp into Titanium surfaces using 2.8 kW laser beam of 186 and 373 MJ m^{-2} energy densities in a nitrogen environment', J. Mater. Process. Technol., 2007, **185**, 38-45.

[26] S. Dyuti, S. Mridha and S.K. Shaha: 'Wear Behavior of Modified Surface Layer Produced by TIG Melting of Preplaced Ti Powder in Nitrogen Environment', Adv. Mat. Research., 2011, **264-265**, 1427-1432.

[27] S. Mridha, A.N.Md Idriss and T.N. Baker: 'Incorporation of TiC particulates on AISI 4340 low alloy steel surfaces via tungsten inert gas arc melting', Adv. Mat. Res., 2012, **445**, 655-660.

[28] W. Kurz: 'Fundamentals of Solidification', 3rd revised ed., Trans Tech. Publication Ltd. Switzerland, 1989, pp.94-6.

[29] R. Colaco, T Carvalho and R. Vilar: 'Laser cladding of stellite 6 on steel substrates', J. High Temp. Chem. Process., 1994, **3(1)**, 21-29.

[30] Ming-xi Li, Yi-zhu He and Guo-xiong Sun: 'Laser cladding Co-based alloy/SiCp composite coatings on IF steel', Mater. Des., 2004, **25**, 355-358.

Table 1: Laser processing conditions.

Sample 1	**Heat input: 125 J mm^{-1}; Speed: 600 mm min^{-1}** **Dilution: 63%**
Sample 2	**Heat input: 188 J mm^{-1}; Speed: 400 mm min^{-1}** **Dilution: 41%**
Power (Output power)	1200 W
Laser waveform	1070 nm
Power feed nozzle angle	0^{O}
Shielding gas (Argon)	10 L min^{-1}
Offset distance	7.24 mm
Spot size	0.96 mm
Powder feed rate/Blown	6 g min^{-1}
Carrier gas	10 L min^{-1}
Etching solution	$HCl+HNO_3$+Glycerol at 1:3:3

Table 2: Gas tungsten arc welding processing conditions.

Sample 3	**Heat input: 1008 J mm^{-1}; Current: 70 A** **Dilution: 87%**
Sample 4	**Heat input: 1296 J mm^{-1}; Current: 90 A** **Dilution: 95%**
Voltage	30 V
Travelling speed	1 mm s^{-1}
Powder application	Preplaced using PVA binder
Powder amount	0.5 mg mm^{-2}
Shielding gas (Argon)	20 L min^{-1}
GTAW electrode	Ø2.4 mm thoriated tungsten
Offset distance	1 mm
Etching solution	Nital

List of Figure Captions:

- Fig. 1: SEM microstructures of the 125 J mm^{-1} laser track showing (a) equiaxed dendrite at the center region, (b) EDX traces from the centre region of the melt pool and (c) columnar dendrites grown from the melt front.

- Fig. 2: SEM microstructures of the 188 J mm^{-1} laser track showing (a) needle like dendrite at the center region, (b) EDX traces from the centre region of the melt pool and (c) a variety of dendrites at the melt front.

- Fig. 3: SEM microstructures of the 1008 J mm^{-1} GTAW track showing (a) fine grain lamellar structure at the center region, (b) EDX traces from the centre region of the melt pool and (c) columnar grains at the melt front.

- Fig. 4: SEM microstructures of the 1296 J mm^{-1} GTAW track showing (a) coarse grain lamellar structure at the center region, (b) EDX traces from the centre region of the melt pool and (c) columnar grains at the melt front.

- Fig. 5: Coated track hardness values for different processing conditions and depths.

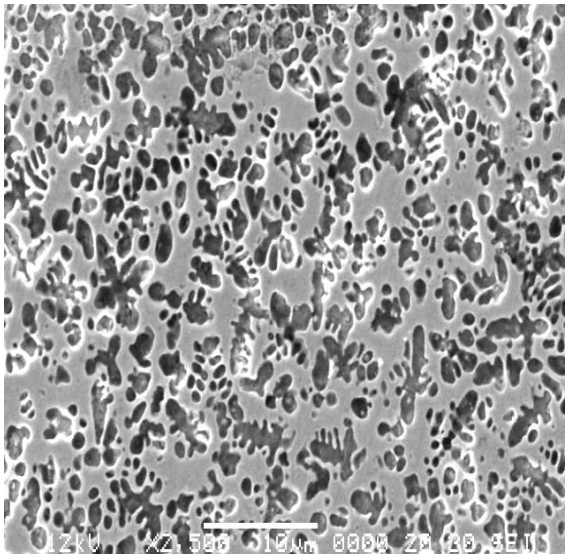

a

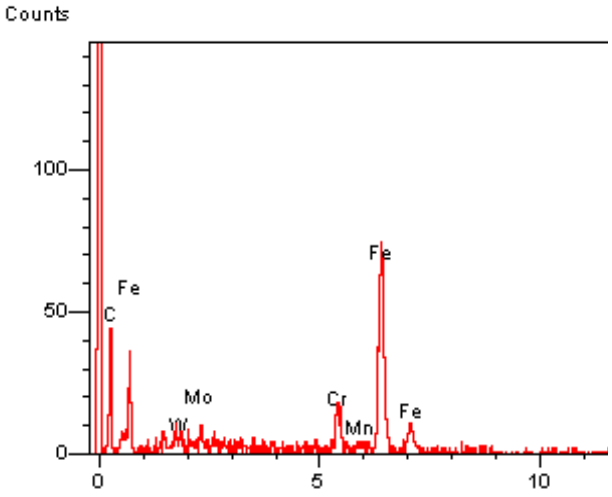

b

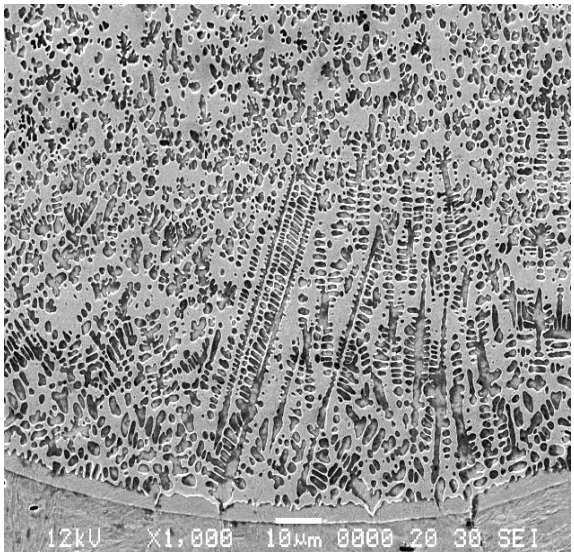

c

Fig. 1: SEM microstructures of the 125 J mm^{-1} laser track showing (a) equiaxed dendrite at the center region, (b) EDX traces from the centre region of the melt pool and (c) columnar dendrites grown from the melt front.

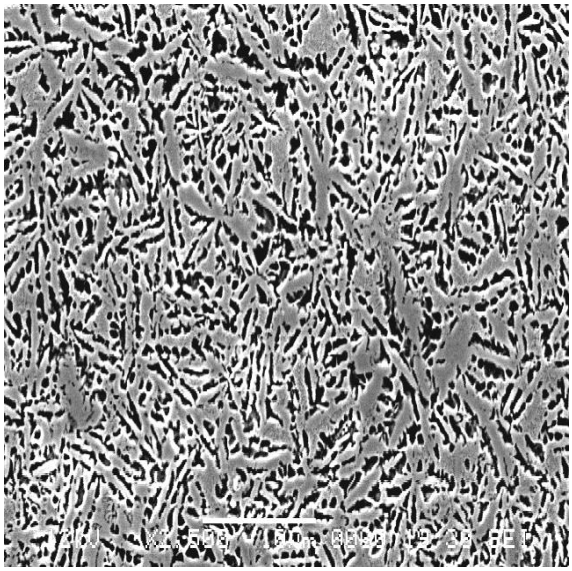

a

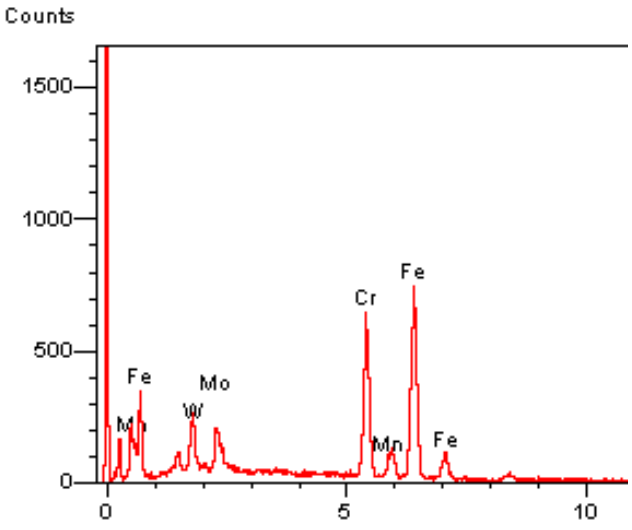

b

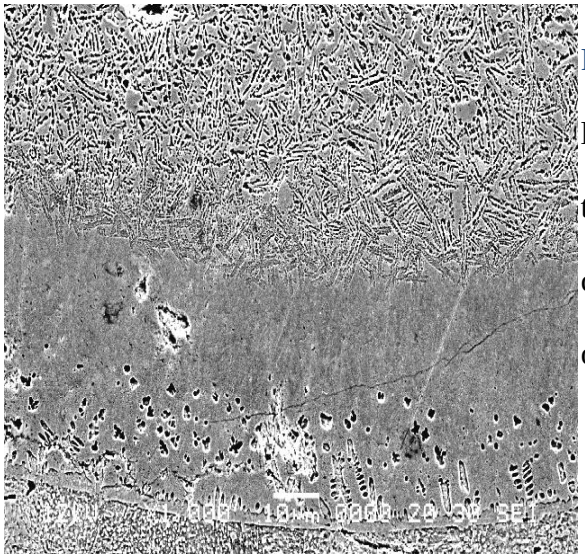

c

Fig. 2: SEM microstructures of the 188 J mm^{-1} laser track showing (a) needle like dendrite at the center region, (b) EDX traces from the centre region of the melt pool and (c) a variety of dendrites at the melt front.

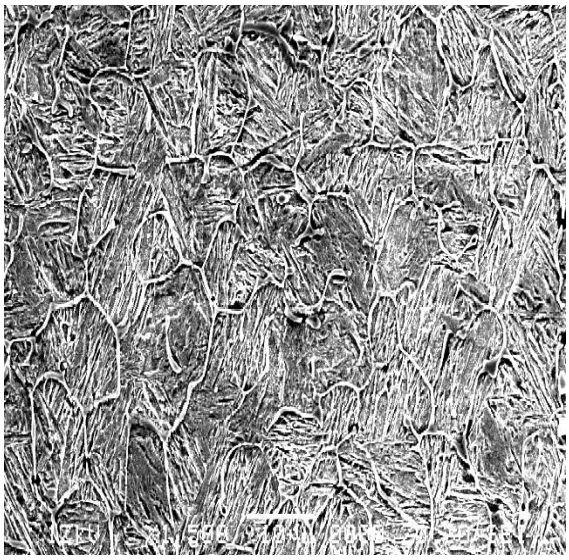

a

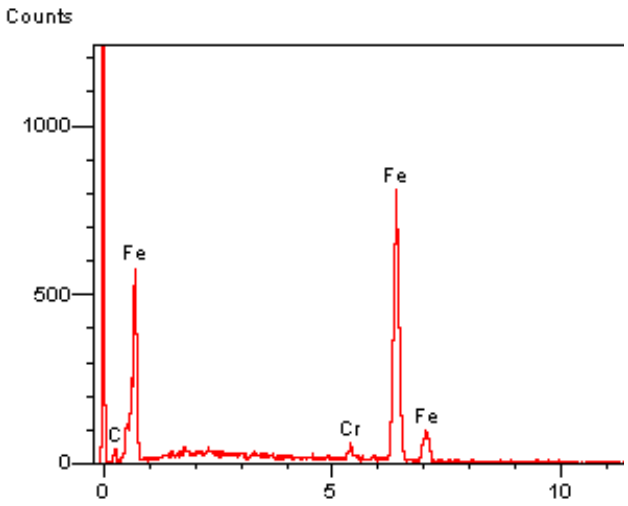

b

c

Fig. 3: SEM microstructures of the 1008 J mm^{-1} GTAW track showing (a) fine grain lamellar structure at the center region, (b) EDX traces from the centre region of the melt pool and (c) columnar grains at the melt front.

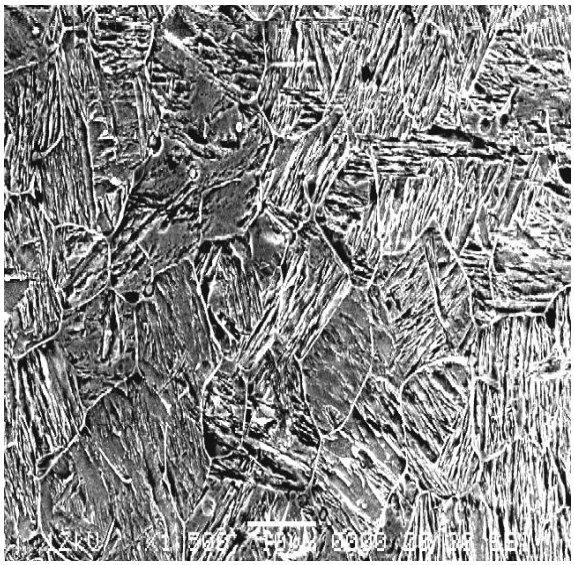

a

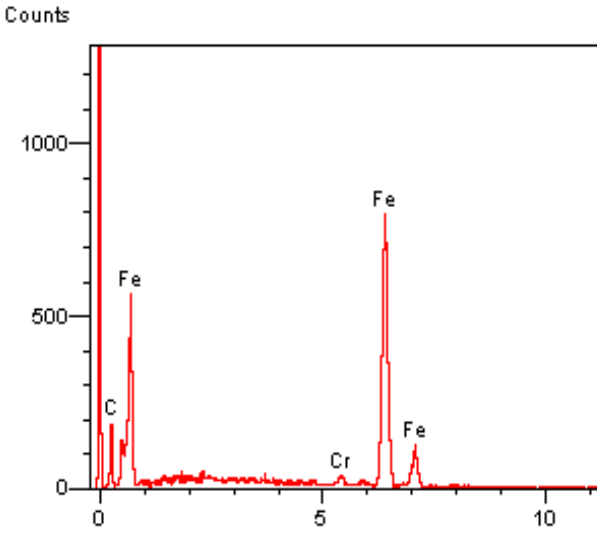

b

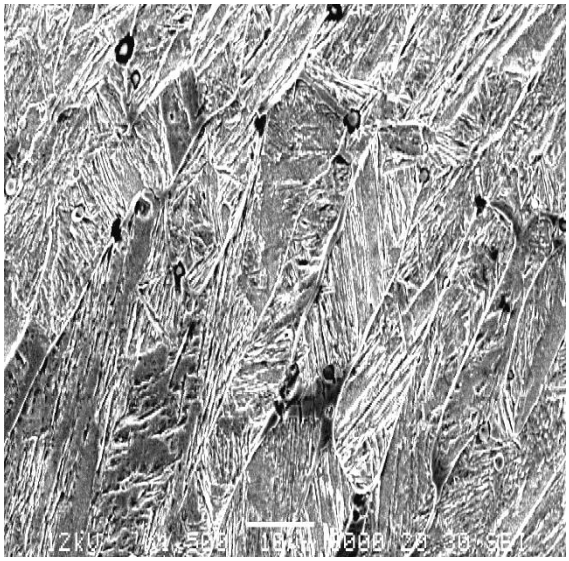

c

Fig. 4: SEM microstructures of the 1296 J mm^{-1} GTAW track showing (a) coarse grain lamellar structure at the center region, (b) EDX traces from the centre region of the melt pool and (c) columnar grains at the melt front.

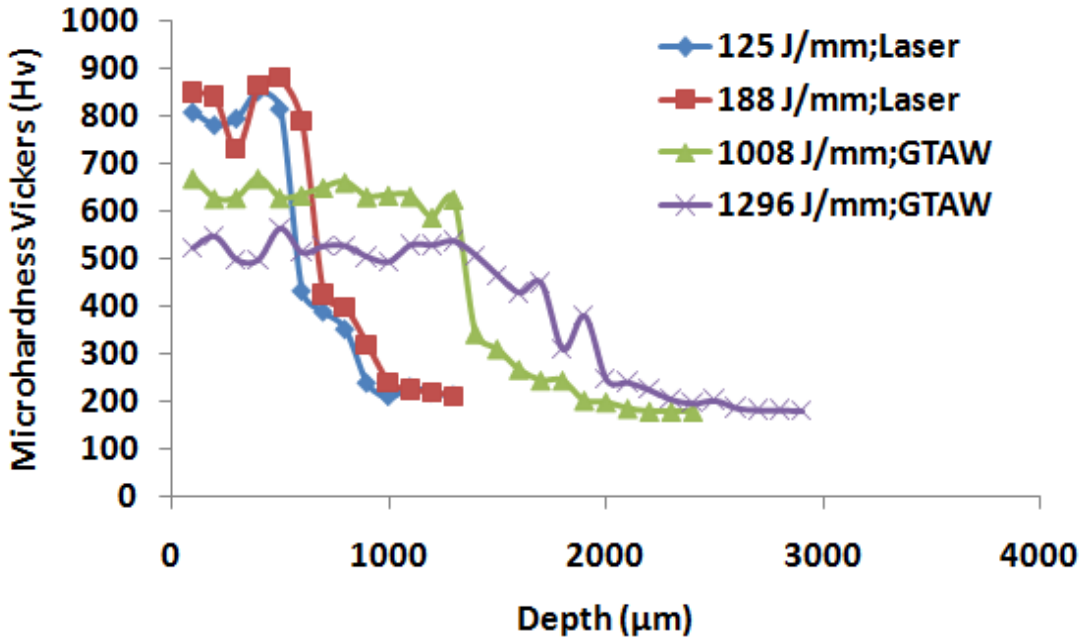

Fig. 5: Coated track hardness values at different processing conditions and depths.